



In-situ SEM observations of ultrasonic cavitation erosion behavior of HVOF-sprayed coatings

Haijun Zhang^a, Xiuyong Chen^{a,b,c,*}, Yongfeng Gong^a, Ye Tian^a, André McDonald^c, Hua Li^{a,b,*}

^a Key Laboratory of Marine Materials and Related Technologies, Zhejiang Key Laboratory of Marine Materials and Protective Technologies, Ningbo Institute of Materials Technology and Engineering, Chinese Academy of Sciences, Ningbo 315201, China

^b Cixi Institute of Biomedical Engineering, Ningbo Institute of Materials Technology and Engineering, Chinese Academy of Sciences, Ningbo 315201, China

^c Department of Mechanical Engineering, University of Alberta, Edmonton, AB T6G 1H9, Canada

ARTICLE INFO

Keywords:

Cavitation erosion
Coatings
Failure mechanism
HVOF
In-situ SEM observation

ABSTRACT

Several typical high-velocity oxy-fuel (HVOF)-sprayed coatings, including WC-10Co4Cr coatings, Co-based coatings, WC-10Co4Cr/Co-based composite coatings, and Fe-based amorphous/nanocrystalline coatings were fabricated, and their cavitation behavior was evaluated in deionized water. Further, *in-situ* SEM surface observations were used to understand the microstructure of tested coatings. The results show that cavitation erosion initially occurred at pre-existing defects in the coatings. Meanwhile, it was found that cavitation erosion damage of the WC-10Co4Cr/Co-based composite coating, which contained a hard reinforcing phase (WC-10Co4Cr phase) and a soft matrix phase (Co-based phase), preferentially occurred at or around pores and microcracks in the reinforcement, rather than in the defect free matrix. This suggested that defects were a critical contributing factor to cavitation damage of the composite coatings. Furthermore, a mechanism was suggested to explicate the cavitation behavior of composite coatings. The approach of using *in-situ* SEM surface observations proved to be useful for the analysis of the cavitation mechanism of engineering materials and protective coatings.

1. Introduction

Cavitation erosion is one of the most common failure modes of flow passage components of ships, fuselage engine fuel systems, and hydraulic systems, such as ship propellers, rudder blades, and centrifugal-chambers [1]. Cavitation is typically caused by the formation, and subsequent collapse, of gas or vapor bubbles in a vibrating liquid or high-speed flow liquid [2,3]. To enhance the cavitation resistant properties of the flow passage components, coating deposition of erosion resistant materials on flow passage component surfaces has been widely adopted. Surface engineering and thermal spraying [4], in particular, high-velocity oxy-fuel (HVOF) has attracted recent attention as a method of fabricating cavitation resistant coatings [5]. HVOF-sprayed coatings have been shown to exhibit properties such as high hardness and low porosity [6], which are necessary features of material removal resistant surfaces. For example, HVOF-sprayed WC-10Co4Cr cermet coatings have been applied on to different industrial parts and are the focus of research on cavitation resistant materials because of its excellent wear resistance, high hardness, improved adhesion to the

virgin component surfaces, and its dense microstructure [7]. In addition, HVOF-sprayed Co-based coatings and Fe-based amorphous/nanocrystalline coatings, which show high hardness, high wear resistance, and corrosion resistance, were widely studied for anti-cavitation applications [5,8]. Nevertheless, the cavitation resistance mechanism of the thermal-sprayed coatings is still unclear. Studying and explaining their cavitation behavior will be essential for and informative on the preparation of high-quality coatings.

To date, many studies have been conducted to investigate the cavitation mechanism of coating materials. These studies have focused on exploring the various defects (porosity [9], microcracks [10], and inter-splat boundaries [11]) and physical properties (fracture toughness [12], hardness [13], adhesion strength [14], and surface roughness [15]) of the coatings as bases for understanding better the cavitation resistance of the coatings. For instance, it was reported that the coating porosity influences the number of initiation points of cavitation erosion damage at the beginning of failure and the fracture toughness has an impact on the propagation speed of cavitation erosion cracks in the coating [7]. It was also noted that pores increased the cavitation damage rate when

* Corresponding authors at: Key Laboratory of Marine Materials and Related Technologies, Zhejiang Key Laboratory of Marine Materials and Protective Technologies, Ningbo Institute of Materials Technology and Engineering, Chinese Academy of Sciences, Ningbo 315201, China.

E-mail addresses: chenxiuyong@nimte.ac.cn (X. Chen), lihua@nimte.ac.cn (H. Li).

<https://doi.org/10.1016/j.ultsonch.2019.104760>

Received 12 June 2019; Received in revised form 12 July 2019; Accepted 29 August 2019

Available online 29 August 2019

1350-4177/ © 2019 Elsevier B.V. All rights reserved.

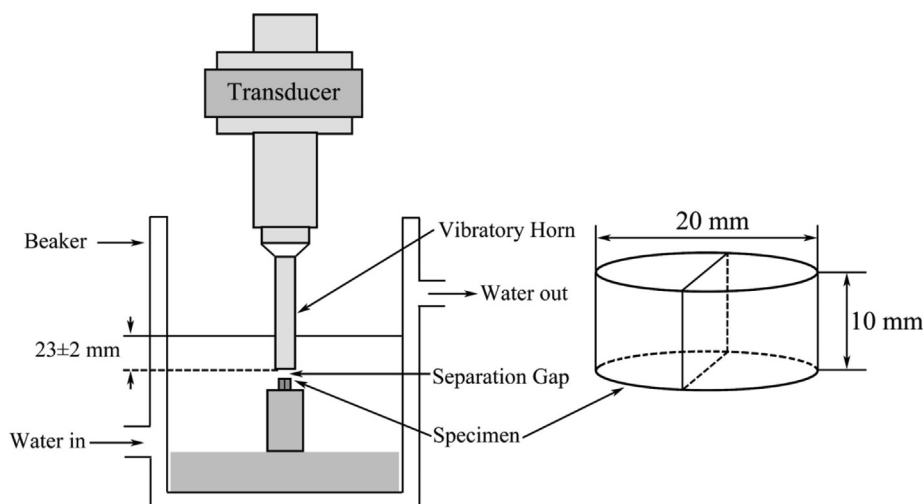


Fig. 1. Schematic diagram of the cavitation erosion test system.

microcracks in the pore region of the surface expanded along the particle boundaries during the cavitation process and fused with the near-surface pores, eventually leading to entire material loss and shedding [16]. However, no study has been reported on the factors that influence damage and material loss (such as defects and the physical properties of the coatings), which plays a more significant role in the cavitation erosion process.

In-situ SEM observation and analysis is a useful strategy to reveal the mechanism of material failure [17–19]. Wang, et al. [17] conducted low cycle fatigue tests to investigate crack initiation and propagation on cast magnesium alloys by using an *in-situ* SEM observation technology. Bouaziz, et al. [18] analyzed coating crack initiation, propagation, and interfacial debonding in tensile tests on nickel-phosphorus (Ni-P) coatings by *in-situ* SEM observation. Zhang, et al. [19] explored the fracture behavior of BT25y alloy (Ti-6.5Al-2Sn-4Zr-5Mo-1W-0.2Si, wt. %) in a tensile loading process at different temperatures by using *in-situ* SEM observations. However, no study has been reported wherein cavitation erosion mechanisms have been investigated using *in-situ* SEM observation and analysis.

In this study, several HVOF-sprayed coatings, including WC-10Co4Cr coatings, Co-based coatings, WC-10Co4Cr/Co-based composite coatings, and Fe-based amorphous/nanocrystalline coatings were prepared on stainless steel substrates. Microstructural and cavitation properties of the coatings were measured. In particular, the mechanism of the cavitation erosion behavior of the HVOF-sprayed coatings was investigated by using *in-situ* SEM observation of the cross-section morphologies of the coatings after different cavitation exposure periods. Based on a review of previous studies, this is the first study that exploits *in-situ* SEM observation to investigate a cavitation erosion mechanism. This study provides a promising technical route for exploring the cavitation mechanism of engineering materials and their protective coatings.

2. Experimental procedure

2.1. Coating preparation

In this study, WC-10Co4Cr powders (Meike thermal spraying technology (Shanghai) Co., Ltd, China), Co-based powders ($\text{Co}_{62.44}\text{Cr}_{27.32}\text{Ni}_{3.01}\text{Si}_{1.33}\text{Mo}_{5.9}$, Shanghai Global Fusion Materials Technology co., Ltd, China), and iron-based powders ($\text{Fe}_{53}\text{Cr}_{19}\text{Zr}_7\text{Mo}_2\text{C}_{18}\text{Si}$, University of Science and Technology Beijing, China) were used as the feedstock powders. WC-10Co4Cr coatings, Co-based coatings, WC-10Co4Cr/Co-based (WC-10Co4Cr + 50 wt% Co) composite coatings, and Fe-based amorphous/nanocrystalline coatings

were fabricated by using a high velocity oxy-fuel (HVOF) spray torch (CJK5, Castolin Eutectic, Germany). The fabrication method has been described in details elsewhere [8,20]. Plates of 316L stainless steel were used as substrates in this study. Before spraying, the substrates were sandblasted with 250 μm (60 mesh) alumina particles, cleaned with acetone, and then dried with warm air.

2.2. Coating characterization

The microstructures of the coatings were studied using a field emission scanning electron microscope (FESEM, FEI Quanta FEG250, USA). The porosities of the coatings were estimated by using an image analysis software (Adobe Photoshop CS6). Ten SEM images of the coatings (cross-sectional view) were used to determine their porosities. The microhardness of the coatings was obtained by using a Vickers hardness indenter (HV-1000, Shanghai Lianer Testing Equipment Co., China) at a test load of 300 g. The mean microhardness value was described based on an average of ten repeated measurements at different locations on the polished cross-section of the coatings.

2.3. Cavitation tests

The cavitation tests were performed by utilizing an ultrasound device (GBS-SCT 20A, Guobiao Ultrasonic Equipment Co., Ltd., Hangzhou, China) with a 1500 W output power, a peak-to-peak amplitude of 50 μm and a 20 kHz output frequency, in accordance with the ASTM G32-16 standard [21]. The schematic of the cavitation erosion equipment is shown in Fig. 1. Before the cavitation erosion tests, the surfaces of the coatings were polished, and for *in-situ* SEM observation, the samples were cut into two equal parts with a cutting machine (SYJ-200, MTI Corporation, USA). The cross-section of the coating was polished to a mirror finish, cleaned with acetone, dried with warm air, and then marked in a specific place to record the original images by SEM. Deionized water was chosen as the test liquid and the vibratory horn was immersed into the water to a depth of 23 mm. The test temperature was maintained at $25 \pm 1^\circ\text{C}$ by circulating fresh water in the cooling bath. The cavitation tests were performed for 35 h in total, with time intervals of 4, 8, 15, 25, and 35 h. The mass losses of the coating samples were recorded after each of cavitation exposure period intervals. After the cavitation tests, all of the coating samples were degreased, rinsed, dried, and then weighed to determine the mass losses. The samples were weighed by using an electronic analytical balance (METTLER 220, TOLEDO Instruments Co., Ltd., Shanghai, China). Each test was repeated three times. The volume loss (V_{loss}) and the rate of volume loss (\dot{V}_{loss}) were used to indicate the cavitation resistance in this

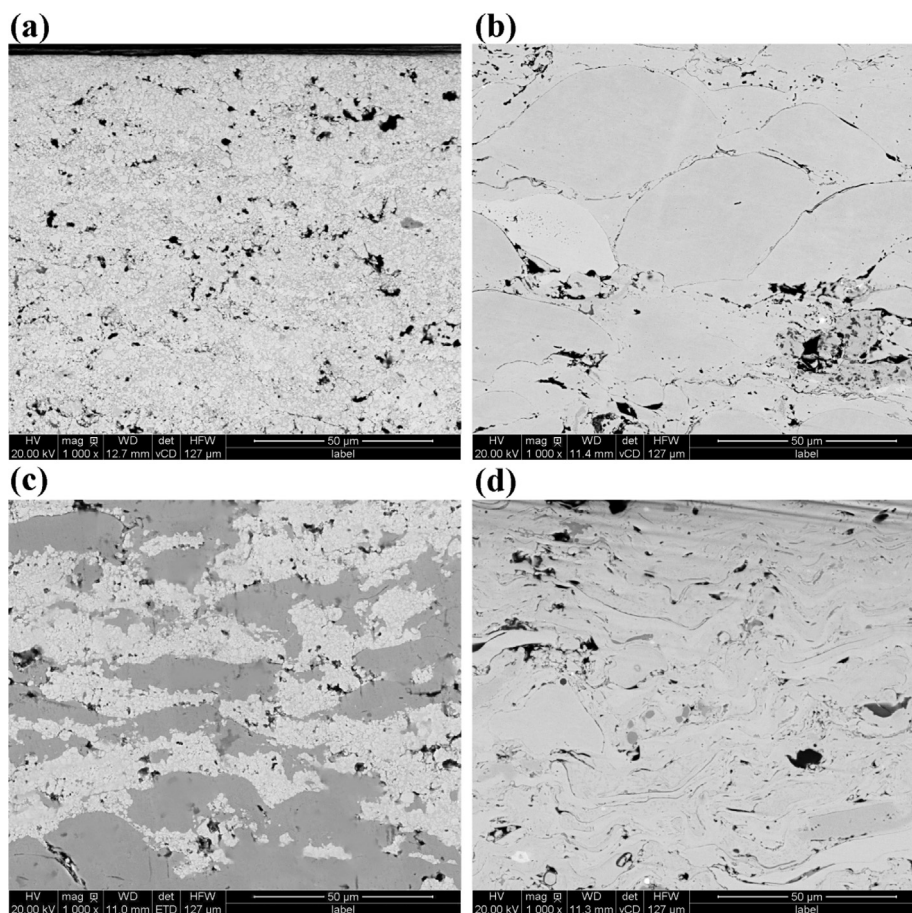


Fig. 2. FESEM cross-sectional morphologies of the (a) WC-10Co4Cr coating, (b) Co-based coating, (c) WC-10Co4Cr/Co-based composite coating, and (d) Fe-based amorphous/nanocrystalline coating.

study. They were calculated according to the equations: $V_{\text{loss}} = \frac{M_{\text{loss}}}{\rho}$ and $\dot{V}_{\text{loss}} = \frac{V_{\text{loss}}}{t}$, respectively, where M_{loss} is mass loss, ρ is the coating density, and t is time. The densities of the coatings were determined according to Archimedes' method. *In-situ* SEM observation was adopted to study the cavitation erosion behavior of the HVOF-sprayed coatings. The microstructure of the cross-section of the coatings after different cavitation exposure periods (4, 8, 15, 25, and 35 h) were observed by using SEM at the same observation point. A control sample that was not exposed to cavitation was also prepared.

3. Results and discussion

3.1. Coating characterization

The microstructure of the coatings was analyzed in order to identify the salient features that would have an impact on the cavitation resistance of the coatings. Fig. 2 shows typical regions of the polished cross-sections of the coatings. The average porosities of these coatings were less than 2.5% (see Table 1), which is consistent with previous

Table 1

Hardness and porosities of the HVOF-sprayed coatings.

Samples	Hardness (HV _{0.3}) (n = 3)	Porosity (%) (n = 3)
WC-10Co4Cr coating	1443.4 ± 121.5	2.2 ± 0.04
Co-based coating	592.8 ± 46.9	0.7 ± 0.03
WC-10Co4Cr/Co-based coating	717.5 ± 73.9	2.1 ± 0.07
Fe-based amorphous/nanocrystalline coating	963.1 ± 74.1	2.3 ± 0.11

studies [22,23]. Pores were observed in the WC-10Co4Cr coatings (Fig. 2a). Cobalt-based coatings, with partially molten particles, were obtained (Fig. 2b). The presence of partially molten particles in the coatings was likely due to the short residence time of the feedstock powder particles in the HVOF spray flame, which in turn led to a rough surface with pores and cracks [24]. The WC-10Co4Cr and Co-based phases were distinctly present in the WC-10Co4Cr/Co-based composite coating (see Fig. 2c). Lamellar structures and some defects (pores) were observed in the Fe-based amorphous/nanocrystalline coating (Fig. 2d). The larger pores were predominantly due to the loose packing of the layered structure of the coating, while the smaller pores in the coating were likely formed during shrinkage porosity, as suggested by Zhou, et al. [25] and Sobolev, et al. [26].

3.2. Failure and material loss due to cavitation

Failure and material loss of the coatings are expected during exposure to the cavitation process. Fig. 3 shows the cumulative volume loss and rates of volume loss of the coatings after cavitation exposure for 35 h in deionized water. The results showed that after 35 h of cavitation erosion, the cumulative volume losses of the WC-10Co4Cr coating, Co-based coating, WC-10Co4Cr/Co-based composite coating, and Fe-based amorphous/nanocrystalline coating were approximately 1.1 mm³, 2.1 mm³, 4.9 mm³, and 6.4 mm³, respectively (see Fig. 3a). All the coating samples experienced volume loss during cavitation exposure, and the losses increased steadily with time during the exposure period. The cavitation erosion resistance was characterized by the volume loss rates, as shown in Fig. 3b, with the WC-10Co4Cr coating presenting with the lowest loss rate and the highest cavitation erosion

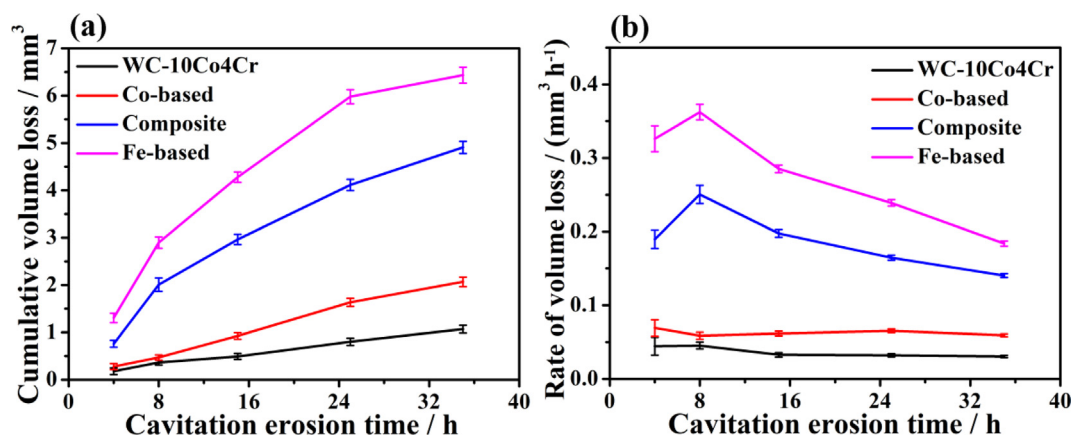


Fig. 3. (a) Cumulative volume loss and (b) rates of volume loss of the WC-10Co4Cr coating, Co-based coating, WC-10Co4Cr/Co-based composite coating, and Fe-based amorphous/nanocrystalline coating after cavitation exposure of 35 h in deionized water.

resistance and the Fe-based amorphous/nanocrystalline coating showing the least resistance. The rate of volume loss of all the coatings that were studied after 8 h cavitation test decreased with cavitation erosion time, and this trend was pronounced in the WC-10Co4Cr/Co-based composite coating and the Fe-based amorphous/nanocrystalline coating. This decreasing rate of volume loss was likely because of the top layers of the coating were removed at the beginning of cavitation exposure due to the relatively looser outer surface microstructure. The superior cavitation resistance of the WC-10Co-4Cr coating was mainly due to the higher microhardness of the coating, as suggested by Kumar, et al. [6]. The low porosity of the Co-based coating was likely a factor that contributed to the relatively good cavitation resistance of that coating system. For the WC-10Co4Cr/Co-based composite coating, the addition of Co-based metallic alloys adversely affected significantly the cavitation performance of the coating. The WC-10Co4Cr/Co-based composite coatings with reduced cavitation resistance were likely due to their lower hardness and higher porosity (Table 1). The Fe-based amorphous/nanocrystalline coating showed the lowest cavitation resistance, and this was due to its high porosity. It is generally known that cavitation erosion resistance increases with increasing hardness or decreasing porosity [27]. Further, cavitation usually initiates at nucleation sites at or around pores and microcracks in coatings [28]. Thus, the presence of these defects will allow for the perpetuation of cavitation erosion and reduction in cavitation erosion resistance.

In-situ SEM observation was performed in the same region of the cross-section surface of the HVOF-sprayed coatings after different cavitation exposure periods to acquire more detailed information on the cavitation behaviors of the coatings in deionized water. Fig. 4 clearly shows the microstructure evolution of the WC-10Co4Cr coating before erosion and as erosion time increased, in particular, the locations highlighted by dashed rectangle and circle. Before the cavitation test, some pores and microcracks were observed (Fig. 4a), which could be preferentially eroded [29,30]. Some eroded zones appeared in the coating after erosion for 4 h (see Fig. 4b). When eroded for 8 h and further for 15 h, the smaller pores tended to be connected because of the exposure to longer periods of cavitation erosion (Fig. 4c and 4d). With further increase of the erosion time to 25 h, and then to 35 h, larger cracks and distinct craters appeared in the cross-sections that were studied (Fig. 4e and 4f). It has been reported that microcracks that initiate at the edge of pre-existing pores and then propagate along with the carbide-binder interface, leading to plastic deformation of proximate material, resulting in the formation of larger cracks and craters due to pulling out of the carbide phase in the coating [7,31]. Additionally, the cobalt-chromium matrix phase might be preferentially removed during erosion and the unsupported WC grains that remain detach as the erosion test time is increased [32]. This is supported by experimental observations shown in Fig. 3a, wherein the cumulative

volume loss of the coating increases with increasing cavitation erosion test time.

For the Co-based coating (Fig. 5), typical defects including pores, partially molten particles, and cracks were observed in the coating before cavitation erosion testing (Fig. 5a). The cracks and the pores gradually connected after eroded for 4 h (Fig. 5b). It was likely due to the presence of the pre-existing pores around the cracks, and the proximate pores and cracks expanded and easily connect together finally under repeated cavitation erosion loading. The sudden collision due to the energetic bursting of bubbles may initiate microcracks. When eroded for 8 h and further to 35 h, as can be seen in Fig. 5c to 5f, additional cracks and craters were observed along with defects created by features such as splat boundaries. It has been reported that cracks preferentially propagate along interlamellar and individual splat boundaries because of the lower cohesive strengths of the coating at these locations [29]. Stress wave propagation will lead to the formation of cracks, and on the other hand, hydraulic penetration will induce enlargement of existing cracks [33]. The failure mode may depend on the toughness of the coating in the later stage of cavitation erosion. Large particles were detached due to the coalescence of fatigue cracks under the coating surface. It was also reported that plastic deformation would cause the enlargement of cracks and form void, and the adjacent voids coalesce, resulting in eventual material loss [34].

For the WC-10Co4Cr/Co-based composite coating (Fig. 6), it could be seen from the as-sprayed composite coating that pores were mainly present in the WC-10Co4Cr phase and microcracks were observed in the Co-based phase (Fig. 6a). As is observed in Fig. 6b–e, the pores and microcracks showed a significant expansion and began to form craters and larger cracks ultimately. Larger craters were formed in the WC-10Co4Cr phase, whereas the extension of microcracks in the Co-based phase was not apparent. This was due to much more defects were present in the WC-10Co4Cr phase than those in the Co-based phase, while damage of the coating usually originated from the defects. Although the WC-10Co4Cr phase possesses excellent physical properties such as high hardness [35], the surface was significantly eroded due to the presence of pores. With further increase of the erosion time to 35 h, larger cavitation craters appeared in the reinforcing particulate phases (WC-10Co4Cr) of the coating by connecting the proximate craters and pores because of the exposure to longer periods of cavitation erosion, while no significant change was observed in the soft matrix phase (Co-based) compared with the result of the erosion time of 25 h (Fig. 6f). The result indicates that defects (such as pores and cracks) in the WC-10Co4Cr/Co-based composite coating were more critical than physical properties (such as hardness) in the cavitation erosion process.

Cracks growth initiated easily at the particle boundaries in the Fe-based amorphous/nanocrystalline coating (see Fig. 7). Some of these cracks were pre-existing in the as-sprayed coating, as shown in Fig. 7a,

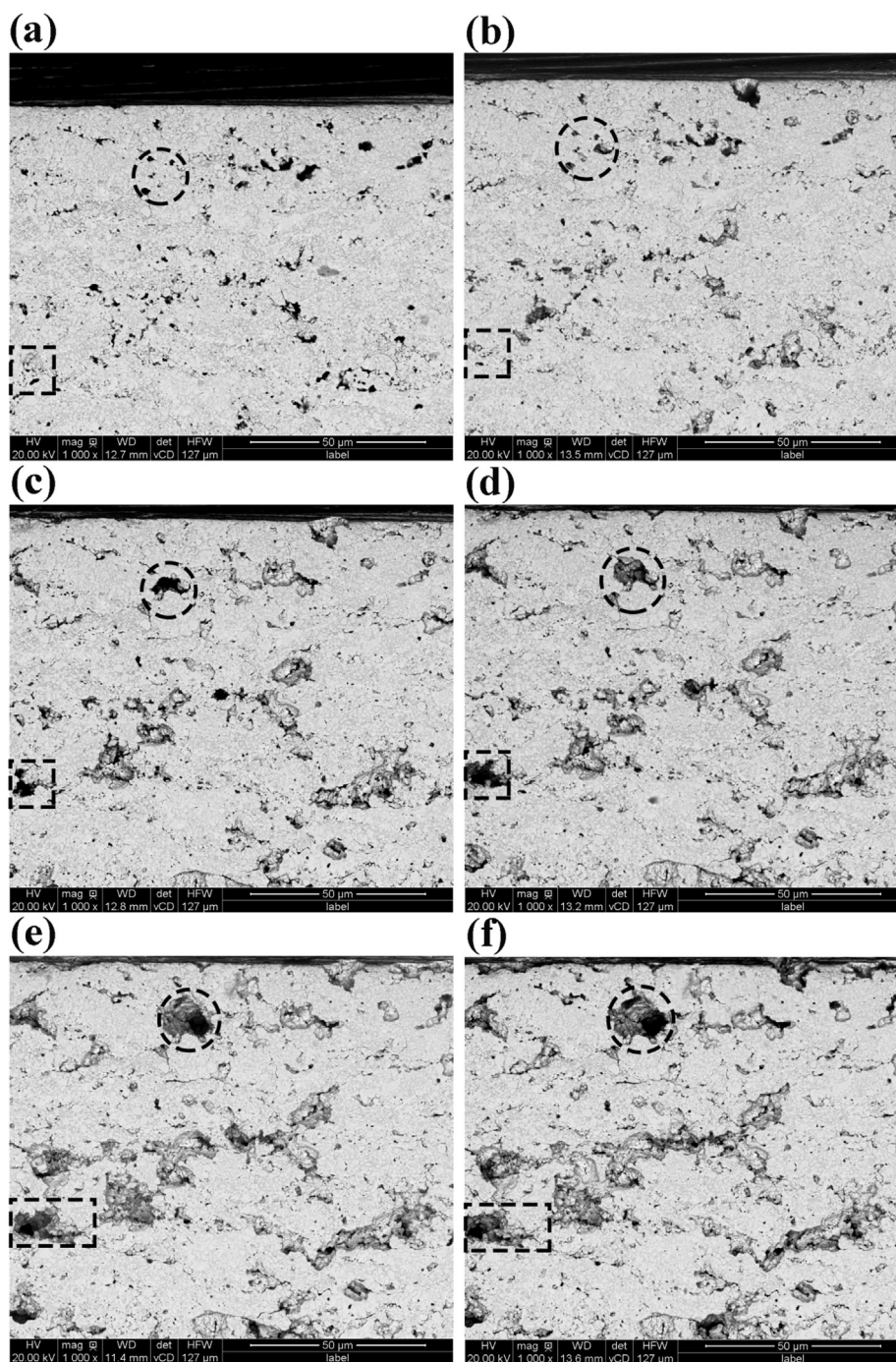


Fig. 4. Typical SEM cross-sectional morphologies of the WC-10Co4Cr coating after (a) 0 h, (b) 4 h, (c) 8 h, (d) 15 h, (e) 25 h, and (f) 35 h of cavitation exposure at the same observation point. A comparison of Fig. 4a–f clearly shows that the pores expanded as erosion time increased. This is highlighted by using dashed rectangles and circles.

with evidence of pores present inside the cracks. It was reported that damage of the Fe-based amorphous/nanocrystalline coating originated from the micro-pores [36]. Pores near the coating surface significantly accelerated the cavitation erosion process via mechanical and chemical erosion. Fig. 7b shows that the pores and microcracks became larger after erosion for 4 h. Under these circumstances, it is hypothesized that the collapse of cavitation bubbles induced the formation of deep cracks that penetrated into the coating. With further increases of the cavitation time to 8 h and then to 25 h, a gradual increase in the size of the craters and cracks occurred (Fig. 7c–e). With the loss of the Fe-based amorphous/nanocrystalline coating material, the pores inside the microcracks gradually became larger and then coalesced to form large cracks

or craters through combination with patulous microcracks during erosion loading. When the cavitation erosion time was increased to 35 h for more aggressive erosion, the microcracks coalesced, and resulted in the detachment of portions of the coating (Fig. 7f)). The microcracks that were initiated at the interfaces between the partially molten particles eventually led to cohesive delamination of the Fe-based amorphous/nanocrystalline coating, as suggested by Qial, et al. [27]. Most of the material loss that occurred may have started at the edges of the particles and the internal splats due to the presence of the partially molten particles and pores around them [16]. In these regions of the coating where abrupt physical changes in the microstructure occurred, it was likely that local stress concentration during erosive loading was

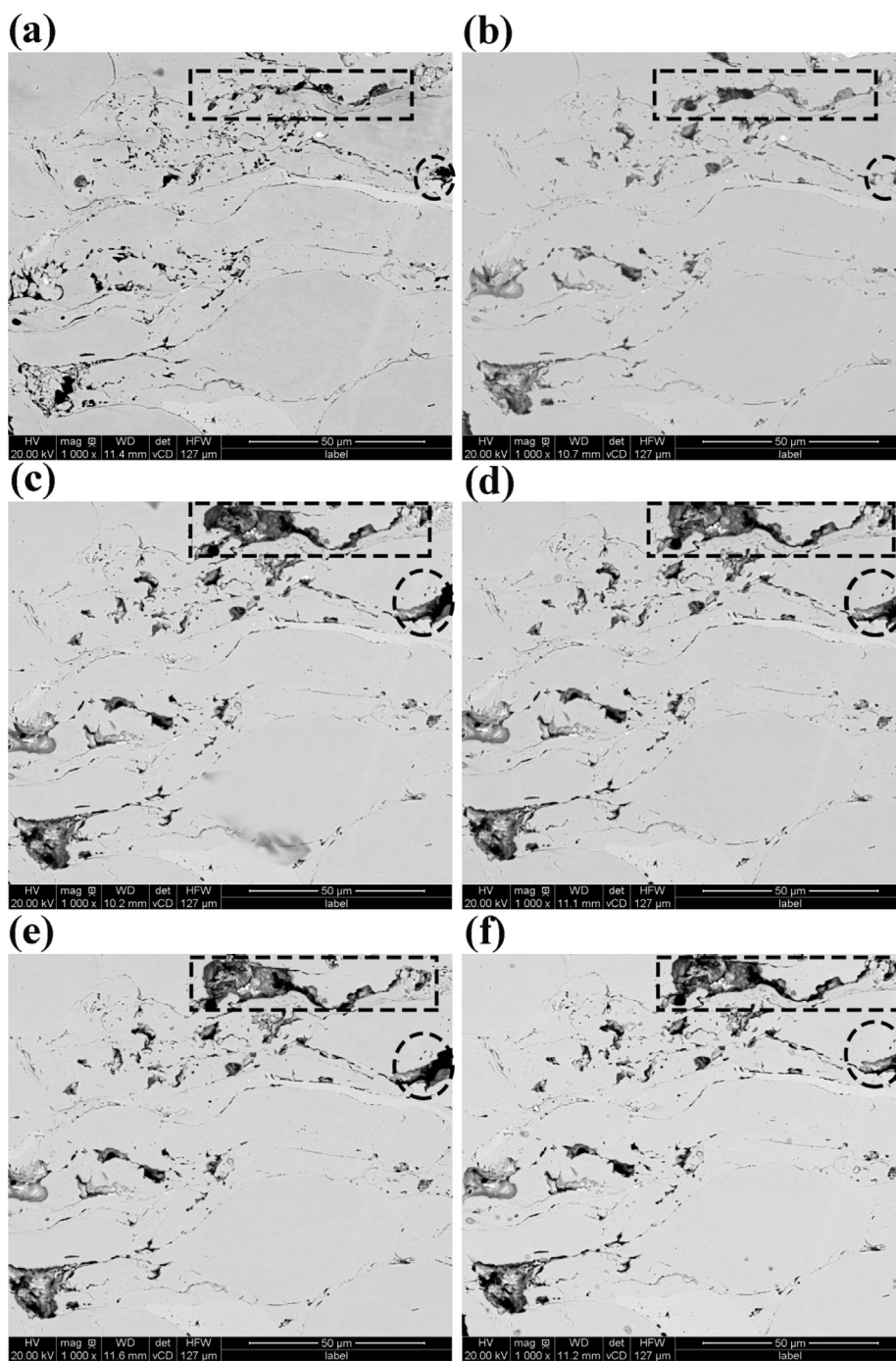


Fig. 5. Typical SEM cross-sectional morphologies of the Co-based coating after (a) 0 h, (b) 4 h, (c) 8 h, (d) 15 h, (e) 25 h, and (f) 35 h of cavitation exposure periods at the same observation point. A comparison of Fig. 5a–f clearly shows that the cracks and pores expanded as erosion time increased. This is highlighted by using dashed rectangles and circles.

sufficient to initiate microcracks and promote crack growth, which eventually led to material loss and coating failure.

3.3. Cavitation failure mechanisms

The *in-situ* SEM analysis that was conducted in this study has enabled elucidation of the failure mechanisms of HVOF-sprayed coatings in deionized water. Fig. 8 presents an illustration of the possible failure mechanisms. Fig. 8a, in particular, corresponds to the original polished surface of the coating, which comprised of a few pores and cracks. The distribution of the pores and cracks are often present in both the matrix and reinforcing particulate phases or at the interface between the

partially molten particles and the fully molten splats. Once the cavitation erosion testing is initiated, the alternating pressure that is caused by ultrasound waves results in the nucleation and collapse of cavitation bubbles, and the formation of defects such as cracks and pores on the surface promote further nucleation, growth, and collapse of bubbles around those defects. Cavitation erosion damage initially occurs at or around pre-existing pores and cracks and then increases during the cavitation erosion process (Fig. 8b). The repeated loading and induced stresses due to shock waves that act on the surface has the noticeable effect of causing the transformation of pores to craters during the cavitation erosion process. The expanded cracks, pores, and craters merge and result in the detachment and loss of coating material under

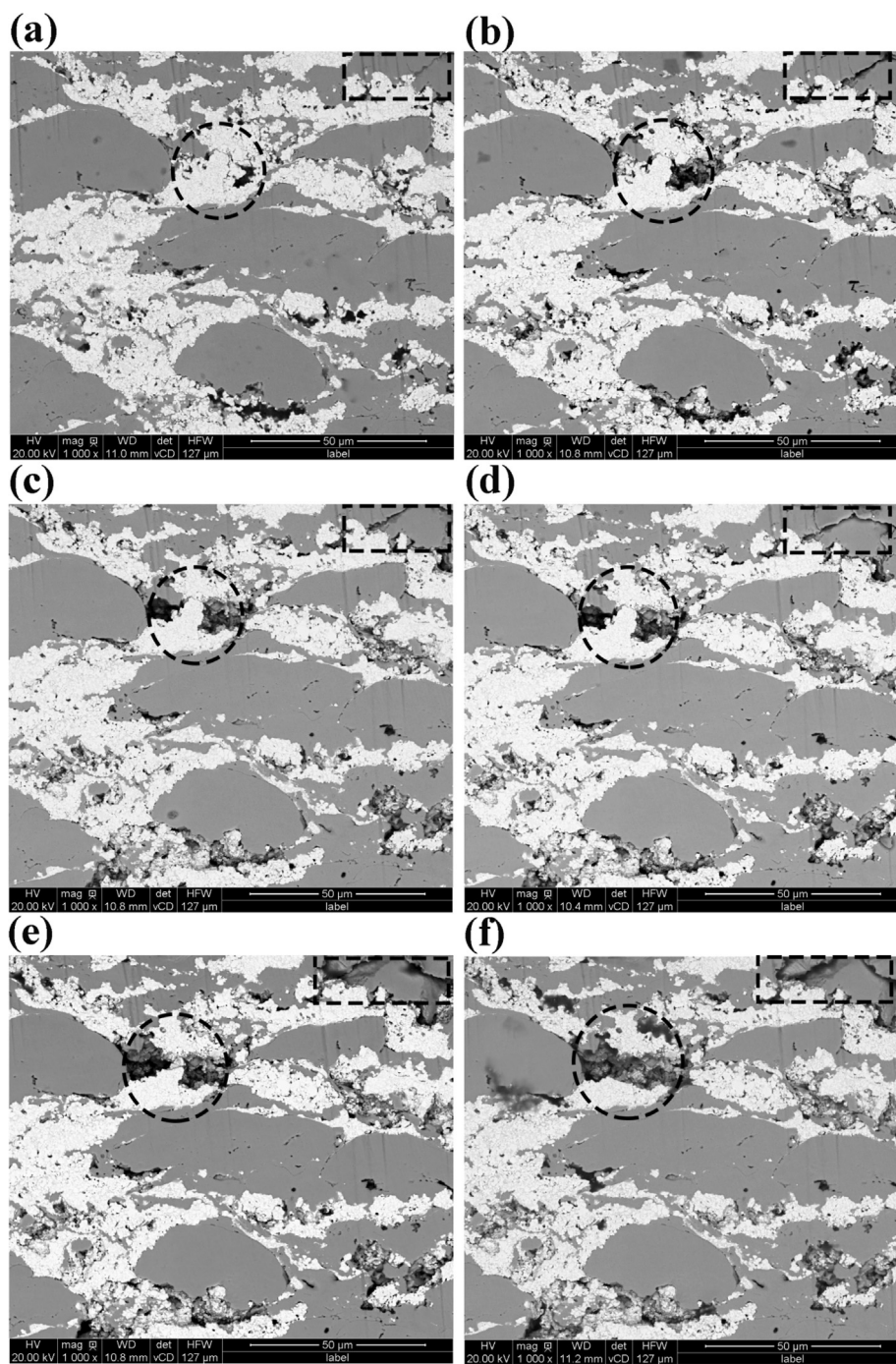


Fig. 6. Typical SEM cross-sectional morphologies of the WC-10Co4Cr/Co-based composite coating after (a) 0 h, (b) 4 h, (c) 8 h, (d) 15 h, (e) 25 h, and (f) 35 h of cavitation exposure periods at the same observation point. A comparison of Fig. 6a–f clearly shows that the cracks and pores expanded as erosion time increased. This is highlighted by using dashed rectangles and circles.

repeated cavitation erosion loading (Fig. 8c). It has been reported that the difference in cavitation erosion rate was mainly due to microstructural features of the coatings [10]. However, it is noteworthy that although the microstructure of the coatings significantly affects the cavitation behavior of the coatings, the final cavitation erosion rates of the coatings appear to be more related to the physical properties of the coating samples in this study, such as hardness. Moreover, and interestingly, in the composite coating with hard reinforcing particulate phases and soft metal matrix phases, cavitation damage is considerably slower in defect-free metal matrix phase areas than in porous hard reinforcing particulate phase areas, as observed from the results shown in Figs. 6 and 8. Taken together, these suggest that the mechanisms of

failure and material loss are significantly influenced by both the presence and coalescence of defects (such as pores and microcracks) in the coatings and their physical properties (such as hardness). More importantly, for composite coatings which contained a hard reinforcing phase and a soft matrix phase, defects were a critical contributing factor to cavitation damage of the coatings over physical properties.

4. Conclusions

- (1) HVOF sprayed WC-10Co4Cr coatings, Co-based coatings, WC-10Co4Cr/Co-based composite coatings, and Fe-based amorphous/nanocrystalline coatings with the porosities of less than 2.5% were

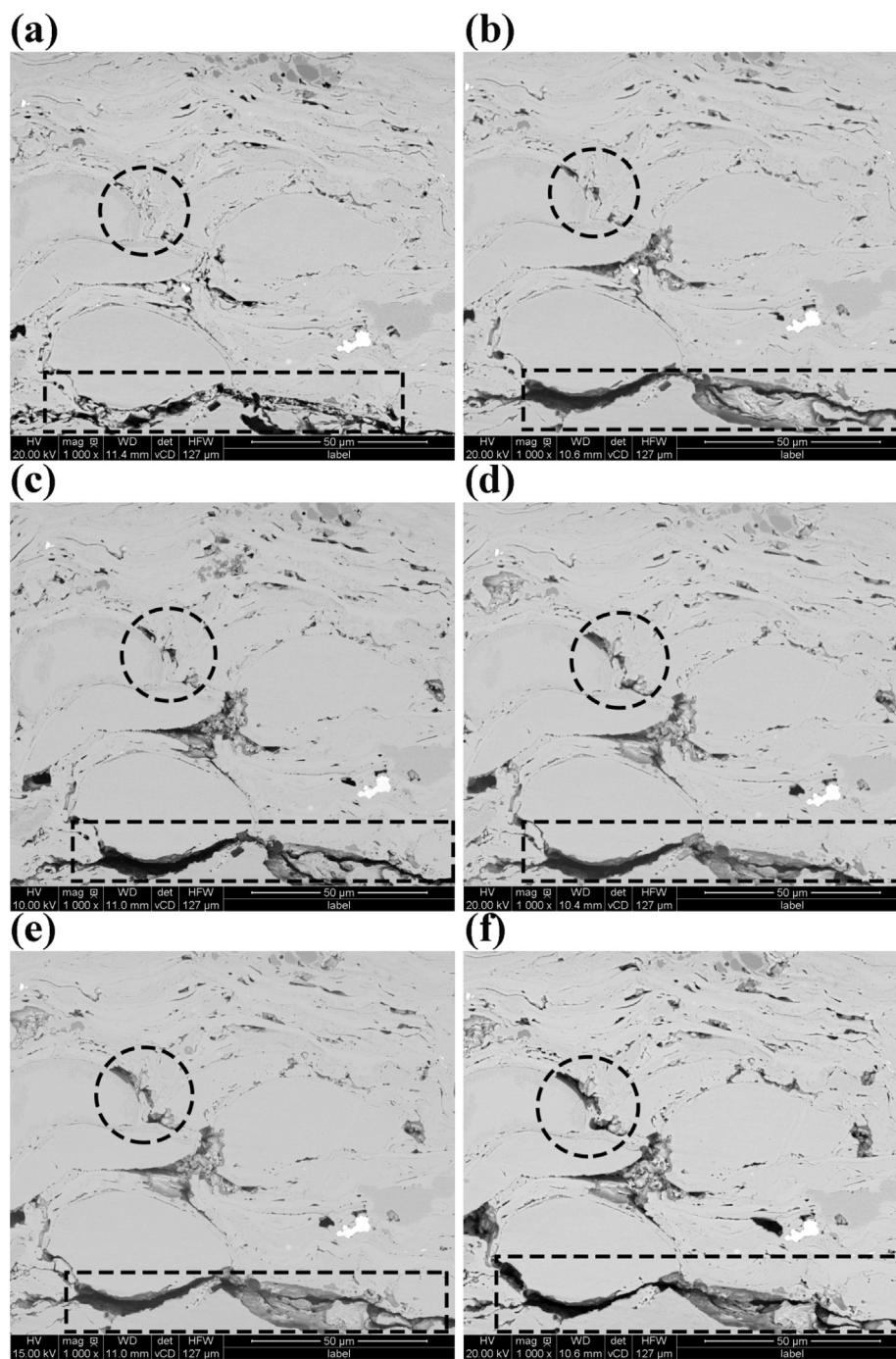


Fig. 7. Typical SEM cross-sectional morphologies of the Fe-based amorphous/nanocrystalline coating after (a) 0 h, (b) 4 h, (c) 8 h, (d) 15 h, (e) 25 h, and (f) 35 h of cavitation exposure periods at the same observation point. A comparison of Fig. 7a–f clearly shows that the cracks and pores expanded as erosion time increased. This is highlighted by using dashed rectangles and circles.

fabricated and their cavitation resistance performances were studied in deionized water. It was found that, amongst the tested coating samples, the WC-10Co4Cr coatings exhibited higher cavitation resistance than those of the other coatings. This was attributed to their unique property of hardness.

(2) It was found that the volume loss rate was greatest at the beginning of the test and then decreased before stabilizing within 8 h for the WC-10Co4Cr coating, while the volume loss rate of the other coatings firstly increased with cavitation erosion time up to 8 h and decreased after that, and this trend was noticeable in the WC-10Co4Cr/Co-based composite coatings and the Fe-based amorphous/nanocrystalline coatings.

(3) The novelty of this work lies in the use of an *in-situ* SEM surface observations method to investigate the cavitation erosion behavior of the coatings, and a mechanism was suggested to illustrate the cavitation behavior of composite coatings. The results demonstrated that microstructural defects (such as cracks and pores) had a significant impact on their cavitation erosion performance because of that the cavitation erosion initiated at or around the pre-existing pores and cracks, and then spread around. More importantly, defects (such as cracks and pores) in composite coatings which contained a hard reinforcing phase and a soft matrix phase were more critical than physical properties (such as hardness) in cavitation erosion. However, future investigations will be needed to assess and

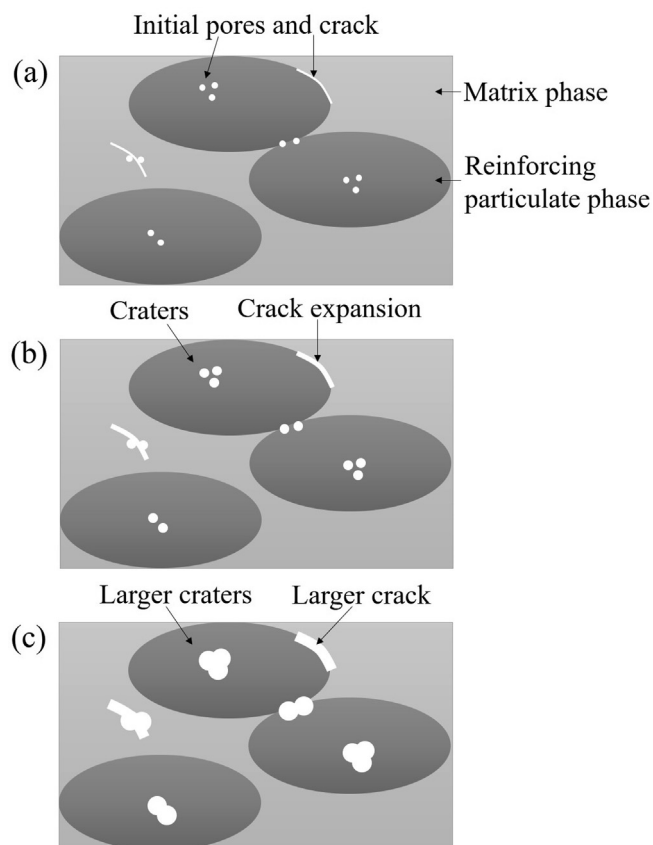


Fig. 8. Schematic diagram of the cavitation erosion process and mechanism.

gain a more detailed understanding of the effects of the coating properties on the cavitation erosion process.

Acknowledgments

This work was supported by the China Scholarship Council (No. 201804910094), CAS-Iranian Vice Presidency for Science and Technology Joint Research Project (grant # 174433KYSB20160085), Chinese Academy of Sciences President's International Fellowship Initiative (grant # 2020VEA0005), National Natural Science Foundation of China (grant # 41706076, 31500772 and 21705158), and a Natural Sciences and Engineering Research Council of Canada Discovery Grant (grant # NSERC RGPIN-2018-04298).

References

- [1] W. Deng, G. Hou, S. Li, J. Han, X. Zhao, X. Liu, Y. An, H. Zhou, J. Chen, A new methodology to prepare ceramic-organic composite coatings with good cavitation erosion resistance, *Ultrason. Sonochem.* 44 (2018) 115–119.
- [2] X. Yang, J. Zhang, G. Li, Cavitation erosion behaviour and mechanism of HVOF-sprayed NiCrBSi-(Cr₃C₂-NiCr) composite coatings, *Surf. Eng.* 34 (2016) 211–219.
- [3] F.T. Cheng, P. Shi, H.C. Man, Correlation of cavitation erosion resistance with indentation-derived properties for a NiTi alloy, *Scr. Mater.* 45 (2001) 1083–1089.
- [4] Z.B. Zheng, Y.G. Zheng, W.H. Sun, J.Q. Wang, Effect of heat treatment on the structure, cavitation erosion and erosion-corrosion behavior of Fe-based amorphous coatings, *Tribol. Int.* 90 (2015) 393–403.
- [5] L. Qiao, Y. Wu, S. Hong, J. Cheng, Ultrasonic cavitation erosion mechanism and mathematical model of HVOF sprayed Fe-based amorphous/nanocrystalline coatings, *Ultrason. Sonochem.* 52 (2019) 142–149.
- [6] R.K. Kumar, M. Kamaraj, S. Seetharamu, T. Pramod, P. Sampathkumaran, Effect of spray particle velocity on cavitation erosion resistance characteristics of HVOF and HVAF processed 86WC-10Co4Cr hydro turbine coatings, *J. Therm. Spray Technol.* 25 (2016) 1217–1230.
- [7] X. Ding, X. Cheng, X. Yu, C. Li, C. Yuan, Z. Ding, Structure and cavitation erosion behavior of HVOF sprayed multi-dimensional WC-10Co4Cr coating, *T. Nonferr. Metal. Soc.* 28 (2018) 487–494.

- [8] H.J. Zhang, Y.F. Gong, X.Y. Chen, A. McDonald, H. Li, A comparative study of cavitation erosion resistance of several HVOF-sprayed coatings in deionized water and artificial seawater, *J. Thermal Spray Technol.* 28 (2019) 1060–1071.
- [9] Y.J. Kim, J.W. Jang, D.W. Lee, S. Yi, Porosity effects of a Fe-based amorphous/nanocrystals coating prepared by a commercial high velocity oxy-fuel process on cavitation erosion behaviors, *Met. Mater. Int.* 21 (2015) 673–677.
- [10] S. Hattori, E. Nakao, Cavitation erosion mechanisms and quantitative evaluation based on erosion particles, *Wear* 249 (2001) 839–845.
- [11] S. Lavigne, F. Pougoum, S. Savoie, L. Martinu, J.E. Klemberg-Sapieha, R. Schulz, Cavitation erosion behavior of HVOF CaviTec coatings, *Wear* 386–387 (2017) 90–98.
- [12] M.S. Lamana, A.G.M. Pukaszewicz, S. Sampath, Influence of cobalt content and HVOF deposition process on the cavitation erosion resistance of WC-Co coatings, *Wear* 398–399 (2018) 209–219.
- [13] P. Zhang, J.H. Jiang, A.B. Ma, Z.H. Wang, Y.P. Wu, P.H. Lin, Cavitation erosion resistance of WC-Cr-Co and Cr₃C₂-NiCr coatings prepared by HVOF, *Adv. Mater. Res.* 15–17 (2006) 199–204.
- [14] C.W. Yang, T.S. Lui, T.M. Lee, E. Chang, Effect of hydrothermal treatment on microstructural feature and bonding strength of plasma-sprayed hydroxyapatite on Ti-6Al-4V, *Mater. Trans.* 45 (2004) 2922–2929.
- [15] J. Lin, Z. Wang, J. Cheng, M. Kang, X. Fu, S. Hong, Effect of initial surface roughness on cavitation erosion resistance of arc-sprayed Fe-based amorphous/nanocrystalline coatings, *Coatings* 7 (2017) 200.
- [16] L.A. Espitia, A. Toro, Cavitation resistance, microstructure and surface topography of materials used for hydraulic components, *Tribol. Int.* 43 (2010) 2037–2045.
- [17] X.S. Wang, C.H. Tan, J. Ma, X.D. Zhu, Q.Y. Wang, Influence of multi-holes on fatigue behaviors of cast magnesium alloys based on *in-situ* scanning electron microscope technology, *Materials* 11 (2018) 1700.
- [18] H. Bouaziz, O. Brinza, N. Haddar, M. Gasperini, M. Feki, *In-situ* SEM study of crack initiation, propagation and interfacial debonding of Ni-P coating during tensile tests: heat treatment effect, *Mater. Charact.* 123 (2017) 106–114.
- [19] W.J. Zhang, X.Y. Song, S.X. Hui, W.J. Ye, *In-situ* SEM observations of fracture behavior of BT25y alloy during tensile process at different temperature, *Mater. Des.* 116 (2017) 638–643.
- [20] D.Y. Li, X.Y. Chen, X.D. Hui, J.P. Wang, P.P. Jin, H. Li, Effect of amorphicity of HVOF sprayed Fe-based coatings on their corrosion performances and contacting osteoblast behavior, *Surf. Coat. Technol.* 310 (2017) 207–213.
- [21] ASTM G32-16, Standard test method for cavitation erosion using vibratory apparatus, *ASTM Int.*, 2016.
- [22] S. Hong, Y.P. Wu, W.W. Gao, B. Wang, W.M. Guo, J.R. Lin, Microstructural characterisation and microhardness distribution of HVOF sprayed WC-10Co-4Cr coating, *Surf. Eng.* 30 (2013) 53–58.
- [23] S. Hong, Y. Wu, Y. Zheng, B. Wang, W. Gao, J. Lin, Microstructure and electrochemical properties of nanostructured WC-10Co-4Cr coating prepared by HVOF spraying, *Surf. Coat. Technol.* 235 (2013) 582–588.
- [24] S.Y. Cui, Q. Miao, W.P. Liang, B.Z. Huang, Z. Ding, B.W. Chen, Slurry erosion behavior of F6NM stainless steel and high-velocity oxygen fuel-sprayed WC-10Co-4Cr coating, *J. Therm. Spray Technol.* 26 (2016) 473–482.
- [25] Z. Zhou, L. Wang, F. Wang, Y. Liu, Formation and corrosion behavior of Fe-based amorphous metallic coatings prepared by detonation gun spraying, *T. Nonferr. Metal. Soc.* 19 (2009) S634–S638.
- [26] V.V. Sobolev, J.M. Guilemany, Investigation of coating porosity formation during high-velocity oxy-fuel (HVOF) spraying, *Mater. Lett.* 18 (1994) 304–308.
- [27] L. Qiao, Y. Wu, S. Hong, J. Zhang, W. Shi, Y. Zheng, Relationships between spray parameters, microstructures and ultrasonic cavitation erosion behavior of HVOF sprayed Fe-based amorphous/nanocrystalline coatings, *Ultrason. Sonochem.* 39 (2017) 39–46.
- [28] R. Fortes Patella, T. Choffat, J.L. Reboud, A. Archer, Mass loss simulation in cavitation erosion: fatigue criterion approach, *Wear* 300 (2013) 205–215.
- [29] Z. Ding, W. Chen, Q. Wang, Resistance of cavitation erosion of multimodal WC-12Co coatings sprayed by HVOF, *T. Nonferr. Metal. Soc.* 21 (2011) 2231–2236.
- [30] N. Ahmed, M.S. Bakare, D.G. McCartney, K.T. Voisey, The effects of microstructural features on the performance gap in corrosion resistance between bulk and HVOF sprayed Inconel 625, *Surf. Coat. Technol.* 204 (2010) 2294–2301.
- [31] S. Hong, Y. Wu, J. Zhang, Y. Zheng, Y. Qin, J. Lin, Ultrasonic cavitation erosion of high-velocity oxygen-fuel (HVOF) sprayed near-nanostructured WC-10Co-4Cr coating in NaCl solution, *Ultrason. Sonochem.* 26 (2015) 87–92.
- [32] F.T. Cheng, C.T. Kwok, H.C. Man, Laser surfacing of S31603 stainless steel with engineering ceramics for cavitation erosion resistance, *Surf. Coat. Technol.* 139 (2001) 14–24.
- [33] A. Guha, R.M. Barron, R. Balachandrar, An experimental and numerical study of water jet cleaning process, *J. Mater. Process. Tech.* 211 (2011) 610–618.
- [34] B.K. Sreedhar, S.K. Albert, A.B. Pandit, Improving cavitation erosion resistance of austenitic stainless steel in liquid sodium by hardfacing-comparison of Ni and Co based deposits, *Wear* 342–343 (2015) 92–99.
- [35] S. Hong, Y. Wu, J. Zhang, Y. Zheng, Y. Qin, W. Gao, G. Li, Cavitation erosion behavior and mechanism of HVOF sprayed WC-10Co-4Cr coating in 3.5 wt% NaCl solution, *Trans. Indian Inst. Metals* 68 (2014) 151–159.
- [36] Z. Wang, X. Zhang, J. Cheng, J. Lin, Z. Zhou, Cavitation erosion resistance of Fe-based amorphous/nanocrystal coatings prepared by high-velocity arc spraying, *J. Therm. Spray Technol.* 23 (4) (2014) 742–749.